SAGE Publishing

Research Article

Highly Selective Separation of C_2H_2/CO_2 and C_2H_2/C_2H_4 in an N-Rich Cage-Based Microporous Metal-Organic Framework

Lingzhi Yang [1,2] **Wenpeng Xie,**[3] **Qiuju Fu,**[3] **Liting Yan,**[1] **Shuo Zhang,**[1,3] **Huimin Jiang,**[1,3] **Liangjun Li,**[3] **Xin Gu,**[3] **Dandan Liu,**[3] **Pengcheng Dai,**[3] **Qingbin Zheng** [2] **and Xuebo Zhao** [1]

[1]*School of Materials Science and Engineering, Qilu University of Technology (Shandong Academy of Sciences), Jinan 250353, China*
[2]*School of Science and Engineering, The Chinese University of Hong Kong, Shenzhen 518172, China*
[3]*Institute of New Energy, College of New Energy, State Key Laboratory of Heavy Oil Processing, China University of Petroleum (East China), Qingdao 266580, China*

Correspondence should be addressed to Qingbin Zheng; zhengqingbin@cuhk.edu.cn and Xuebo Zhao; zhaoxuebo@upc.edu.cn

The separation of acetylene (C_2H_2) from carbon dioxide (CO_2) and the purification of ethylene (C_2H_4) from C_2H_2 are quite essential processes for the chemical industry. However, these processes are challenging due to their similar physical properties, including molecule sizes and boiling points. Herein, we report an N-rich cage-based microporous metal-organic framework (MOF), $[Cd_5(Tz)_9](NO_3)$ (termed as Cd-TZ, TZ stands for tetrazole), and its highly efficient separation of C_2H_2/CO_2 and C_2H_2/C_2H_4. Single-component gas adsorption isotherms reveal that Cd-TZ exhibits high C_2H_2 adsorption capacity (3.10 mmol g^{-1} at 298 K and 1 bar). The N-rich cages in Cd-TZ can trap C_2H_2 with a higher isosteric heat of adsorption (40.8 kJ mol^{-1}) than CO_2 and C_2H_4 owing to the robust host-guest interactions between the noncoordinated N atoms and C_2H_2, which has been verified by molecular modeling studies. Cd-TZ shows a high IAST selectivity for C_2H_2/CO_2 (8.3) and C_2H_2/C_2H_4 (13.3). The breakthrough simulations confirm the potential for separating C_2H_2/CO_2 and the purification of C_2H_4 from C_2H_2.

1. Introduction

C_2H_2 and C_2H_4 are two of the most important chemical raw feedstocks for producing various commercial chemicals [1]. C_2H_2 is mainly obtained from coal or coal-derived coke with direct or indirect processes [2]. Thus, CO_2 is usually contained in the crude acetylene as an unavoidable impurity generally removed in an aqueous sodium hydroxide wash. C_2H_2 can also be purified by dissolving in organic solvents, such as N-methylpyrrolidone and dimethylformamide. C_2H_4 is typically produced by the pyrolysis of ethane gas or light naphtha, with a small amount of C_2H_2 generated. C_2H_2 in mixtures must be removed, reducing its content to below 5 ppm [3, 4] because of the effects of C_2H_2 in poisoning catalysis during the polymerization process of ethylene. Solvent extraction and partial hydrogenation are the main

commercial techniques to separate trace C_2H_2 from C_2H_4. However, both the purification methods of C_2H_2 and C_2H_4 used in the chemical industry are with poor separation selectivity and are energy-intensive [5]. Alternatively, selective adsorption and separation processes based on porous sorbents are energy-efficient and sustainable.

In recent decades, MOFs [6–12] have been studied widely in separations and purifications for hydrocarbons [13–24]. However, the molecular sizes ($3.3 \times 3.3 \times 5.7$ Å^3 for C_2H_2, $3.2 \times 3.3 \times 5.4$ Å^3 for CO_2, and $3.3 \times 4.2 \times 4.8$ Å^3 for C_2H_4) and kinetic diameter (3.3 Å for C_2H_2, 3.3 Å for CO_2, and 4.2 Å for C_2H_4) of acetylene, carbon dioxide, and ethylene are very close [7, 25], making the efficient separation of C_2H_2/CO_2 and C_2H_2/C_2H_4 a challenge. Until now, MOFs [7, 26–31] with highly selective separation

performance for both C_2H_2/CO_2 and C_2H_2/C_2H_4 are still rare. Currently, the reported MOF materials with record selectivity for C_2H_2/CO_2 and C_2H_2/C_2H_4 is an anion-pillared flexible MOF, UTSA-300a [26]. Because of the strong C–H···F hydrogen-bonding interaction between UTSA-300a and C_2H_2, C_2H_2 can easily open the pore and be adsorbed into it while the other gases are blocked out of the pore. Lee and co-workers [28] reported a cationic MOF, JCM-1, which possesses imidazolium and nitrate groups in the pore channel, exhibiting a higher selectivity and adsorption affinity for C_2H_2 than for CO_2 or C_2H_4. A broad strategy in MOFs to enhance the selectivity of C_2H_2/CO_2 and C_2H_2/C_2H_4 is to increase the polar groups or adsorption sites, such as fluorine/nitrogen/oxygen-containing functional groups, to strengthen the interaction with C_2H_2 over CO_2 or C_2H_4.

Herein, we report a microporous MOF $[Cd_5(Tz)_9](NO_3)$ [32] with N-rich cavities for the preferential adsorption of C_2H_2 and the efficient separation for C_2H_2/CO_2 and C_2H_2/C_2H_4. At ambient conditions, Cd-TZ shows a higher adsorption capacity and isosteric heat of adsorption for C_2H_2 than for CO_2 and C_2H_4. Thus, Cd-TZ exhibits elevated C_2H_2/CO_2 and C_2H_2/C_2H_4 selectivity. The modeling studies reveal that the trapped C_2H_2 molecule is in the center of the cavity and strongly interacts with the surrounding N atoms. The simulated breakthrough curves demonstrate the effective separation of binary mixtures of C_2H_2/CO_2 and C_2H_2/C_2H_4.

2. Materials and Methods

2.1. Materials.
All reagents and solvents were commercially available and, unless otherwise noted, were used without further purification. Cadmium nitrate tetrahydrate ($Cd(NO_3)_2 \cdot 4H_2O$, AR) was purchased from Aladdin Reagent Co. Ltd. Ethyl tetrazole-5-carboxylate (>95%) was purchased from Bidepharm Co. Ltd.

High-purity CO_2 (99.999%), C_2H_4 (99.95%), and C_2H_2 (99.9%) were purchased from Qingdao Tianyuan Gas Co., Ltd. C_2H_2 was filtered through activated carbon to remove traces of acetone before use.

2.2. Synthesis of Cd-TZ.
Cd-TZ was synthesized according to the methods reported in the literature [32]. A mixture of $Cd(NO_3)_2 \cdot 4H_2O$ and ethyl tetrazole-5-carboxylate was dissolved in 10 mL H_2O, then transferred to a 23 mL Teflon-lined autoclave and heated at 433 K for 72 h, followed by cooling to room temperature. Colorless crystals were collected by filtration and washed with H_2O and methanol. The activation process of the Cd-TZ sample was conducted under a vacuum at 423 K for 12 h.

2.3. Characterizations of Cd-TZ.
Thermogravimetric analyses (TGA) were examined using a Netzsch STA 449C instrument under an N_2 atmosphere with a heating rate of 5 K min^{-1}. Powder X-ray diffraction (PXRD) data were performed on an X-ray diffractometer (Bruker D8 Adv., Germany) with Cu Kα radiation from 5 to 50° ($\lambda = 1.5406$) and a step size of 0.0167° in 2θ.

2.4. Adsorption Studies for CO_2, C_2H_2, and C_2H_4.
The sample was degassed in a vacuum for 12 h at 423 K to remove guest molecules before adsorption. Equilibrium and kinetic adsorption experiments of CO_2, C_2H_2, and C_2H_4 were measured using a XEMIS magnetic suspension balance sorption analyzer (Hiden, UK) equipped with a circulating water bath at 273 K and 298 K, respectively.

2.5. Calculation of Brunauer-Emmett-Teller (BET) Surface Area and Langmuir Surface Area.
Surface areas of Cd-TZ were calculated using the BET equation and Langmuir equation based on the CO_2 adsorption isotherm at 273 K.

BET surface area:

$$\frac{P}{n(P_0 - P)} = \frac{1}{C\,n_m} + \frac{C-1}{C\,n_m} \cdot \frac{P}{P_0}, \tag{1}$$

$$S_{\text{BET}} = n_m \cdot A \cdot \sigma_m. \tag{2}$$

Langmuir surface area:

$$\frac{P}{n} = \frac{P}{n_m} + \frac{1}{b\,n_m}, \tag{3}$$

$$S_{\text{Langmuir}} = n_m \cdot A \cdot \sigma_m, \tag{4}$$

where P is the pressure (bar), P_0 is the saturated vapor pressure, n is the adsorption amount under the corresponding pressure, n_m is the amount related to the monolayer surface coverage, C ($C > 0$) and b are constants, σ_m is the cross-sectional area of CO_2 (2.18×10^{-19} m^2), and S_{BET} and S_{Langmuir} are the calculated BET surface area and Langmuir surface area, respectively.

2.6. Calculation of Isosteric Enthalpy of Adsorption.
Isosteric enthalpy of adsorption (Q_{st}) was calculated from isotherms measured at 273 K and 298 K for CO_2, C_2H_2, and C_2H_4. The isotherms were firstly fit to a virial equation:

$$\ln P = \ln N + \frac{1}{T} \sum_{i=0}^{m} a_i N^i + \sum_{i=0}^{n} b_i N^i, \tag{5}$$

where P is the pressure expressed in mbar, N is the amount adsorbed in mmol g^{-1}, T is the temperature in K, a_i and b_i are virial coefficients, and m and n represent the number of coefficients required to describe the isotherms adequately. To calculate Q_{st}, the fitting parameters from the above equation were used for the following equation:

$$Q_{\text{st}} = -R \sum_{i=0}^{m} a_i N^i. \tag{6}$$

2.7. Ideal Adsorbed Solution Theory (IAST) Selectivity Calculation.
The gas adsorption isotherms were firstly fitted to a dual-site Langmuir-Freundlich (DSLF) equation:

$$q = q_1 \frac{b_1 p^{n_1}}{1 + b_1 p^{n_1}} + q_2 \frac{b_2 p^{n_2}}{1 + b_1 p^{n_2}}, \tag{7}$$

where q (mmol g^{-1}) is the amount of adsorbed gas; p (mbar) is the bulk gas phase pressure; q_1 (mmol g^{-1}) and q_2 (mmol g^{-1}) are the saturation capacities of sites 1 and 2, respectively; b_1 (mbar^{-n1}) and b_2 (mbar^{-n2}) are the affinity coefficients of site 1 and site 2, respectively; and n_1 and n_2 represent the deviations from an ideal homogeneous surface.

The adsorption selectivity is defined by

$$S_{ads} = \frac{x_1/y_1}{x_2/y_2}, \tag{8}$$

where x_i and y_i are the mole fractions of component i ($i = 1$ and 2) in the adsorbed and bulk phases, respectively.

2.8. Density-Functional Theory Calculations. All the geometry optimizations and binding energies were calculated by the periodic density functional theory (DFT) method using the DMol^3 module. The host framework and the gas molecule were both regarded as rigid. The structures of the framework were first optimized. Then, guest gas molecules were introduced to the optimized framework, followed by a full structure relaxation. An isolated gas molecule placed in a supercell (with the same cell dimensions as the framework) was also relaxed as a reference to obtain the gas binding energy. The widely used generalized gradient approximation (GGA) with the Perdew-Burke-Ernzerhof (PBE) functional and the double numerical plus polarization (DNP) basis set, the Grimme method for DFT-D correction, and the DFT semicore pseudopots (DSPP) were used. The energy, force, and displacement convergence criteria were set as 1×10^{-5} Ha, 2×10^{-3} Ha, and 5×10^{-3} Å, respectively. The following equations then calculated the static binding energy (at $T = 0$ K):

$$\Delta E_{binding} = E_{MOF} + E_{gas} - E_{(MOF+gas)}, \tag{9}$$

where $\Delta E_{binding}$ is the static binding energy between the MOF and the gas molecule and E_{MOF}, E_{gas}, and $E_{(MOF+gas)}$ are the energies of the gas-free MOF, the free gas molecule, and the MOF-gas system, respectively.

2.9. Breakthrough Simulation. Breakthrough simulations were performed using the 3P-Sim software. In the simulated separation experiment, the Cd-TZ (1.0 g) was packed into the column with a length of 5 cm and an inner diameter of 0.45 cm. And the simulated operating condition is under 1 bar at 298 K with a continuous gas (C_2H_2/CO_2 (50/50, v/v) or C_2H_2/C_2H_4 (50/50, v/v)) flow of 2 mL (STP) min^{-1}.

3. Results and Discussion

As shown in Figures 1(a) and 1(b), each Cd (II) atom in the framework is surrounded by different tetrazole ligands and coordinated with six nitrogen atoms to form an octahedral coordination structure, resulting in a cationic three-dimensional framework $[Cd_5(Tz)_9]^+$ which is balanced by NO_3^-. Cd (II) atoms interconnect such six second-building units to form one-dimensional straight pore channels (4.6 Å), which have large cavities (5.3 Å) parallel to each

other along the c axis (Figures 1(c) and 1(d)). The surface of the cavities contains many uncoordinated tetrazole nitrogen atoms, which is conducive to capturing C_2H_2 molecules. Cd-TZ was successfully prepared by hydrothermal reaction at 433 K, and the phase purity of the material was identified by PXRD patterns which nicely match the calculated patterns from single crystal data (Figure 2(a)). To investigate the thermal stability of Cd-TZ, the synthesized Cd-TZ samples were subjected to TGA under a nitrogen atmosphere, as shown in Figure 2(b). The TGA curves show that the Cd-TZ sample lost most of the free water molecules in the pore channels as the temperature increased to 98°C. When the temperature exceeded 300°C, the sample lost weight rapidly. This phenomenon indicates that Cd-TZ has good thermal stability under a nitrogen atmosphere and can maintain the structure over a wide temperature range (<300°C). The specific surface area of Cd-TZ was characterized using CO_2 adsorption experiments performed at 273 K (Figure S1a). And the BET surface area (Figure S1b) and Langmuir surface area (Figure S2) were calculated to be 388 m^2 g^{-1} and 403 m^2 g^{-1}, respectively.

Considering the suitable pore size and the presence of abundant uncoordinated nitrogen atoms in the pore surface of Cd-TZ, we were intrigued to explore its potential to capture C_2H_2 and, further, to separate C_2H_2/CO_2 and C_2H_2/C_2H_4. Therefore, single-component adsorption-desorption isotherms of C_2H_2, CO_2, and C_2H_4 were collected at 273 K and 298 K (Figures 3(a) and 3(b)). The adsorption capacity of C_2H_2 is higher than those of CO_2 and C_2H_4 in Cd-TZ under the same conditions. The C_2H_2 capacity is 3.10 mmol g^{-1} at 298 K and 1 bar, higher than the capacity of CO_2 (2.07 mmol g^{-1}) and C_2H_4 (1.68 mmol g^{-1}) and outperforming many reported MOFs, such as ZU-62-Ni (3.0 mmol g^{-1}) [33], NKMOF-1-Ni (2.7 mmol g^{-1}) [34], Zn(ad)(int) (2.32 mmol g^{-1}) [35], CPL-1-NH$_2$ (1.84 mmol g^{-1}) [36], and Zn-FBA (1.03 mmol g^{-1}) [37]. Furthermore, the C_2H_2 adsorption isotherms rise rapidly in the low-pressure region at 273 K and 298 K. At 298 K and 0.01 bar, the uptake ratio of C_2H_2/CO_2 and C_2H_2/C_2H_4 in Cd-TZ is 1.8 and 3.0, respectively, indicating the stronger interaction between C_2H_2 and Cd-TZ. The isosteric enthalpies of adsorption for C_2H_2, CO_2, and C_2H_4 were calculated based on fitting using the virial method (Figure S3-S5) to evaluate the interaction between the framework and the guest molecule. As shown in Figure 3(c), the calculated value of Q_{st} for C_2H_2, CO_2, and C_2H_4 at zero loading is 40.8 kJ mol^{-1}, 35.6 kJ mol^{-1}, and 31.8 kJ mol^{-1}, respectively. Furthermore, the Q_{st} value of Cd-TZ for C_2H_2 is higher than those for CO_2 and C_2H_4 over the entire pressure range from 0 to 1 bar. All the results demonstrate that Cd-TZ prefers to adsorb C_2H_2 and has a stronger affinity for C_2H_2 than CO_2 and C_2H_4, which prompts us to explore the separation performance of Cd-TZ for the binary gas of C_2H_2/CO_2 and C_2H_2/C_2H_4.

The adsorption selectivity for C_2H_2/CO_2 (50/50, v/v) and C_2H_2/C_2H_4 (50/50, 1/99, v/v) was calculated based on the IAST model based on fitting using the DSLF equation (Figure S6-S8). The selectivity of Cd-TZ for C_2H_2/CO_2 (50/50, v/v) is 8.3 at 298 K and 1.0 bar (Figure S9), which is compared to the reported UTSA-74a (9.0) [38], and
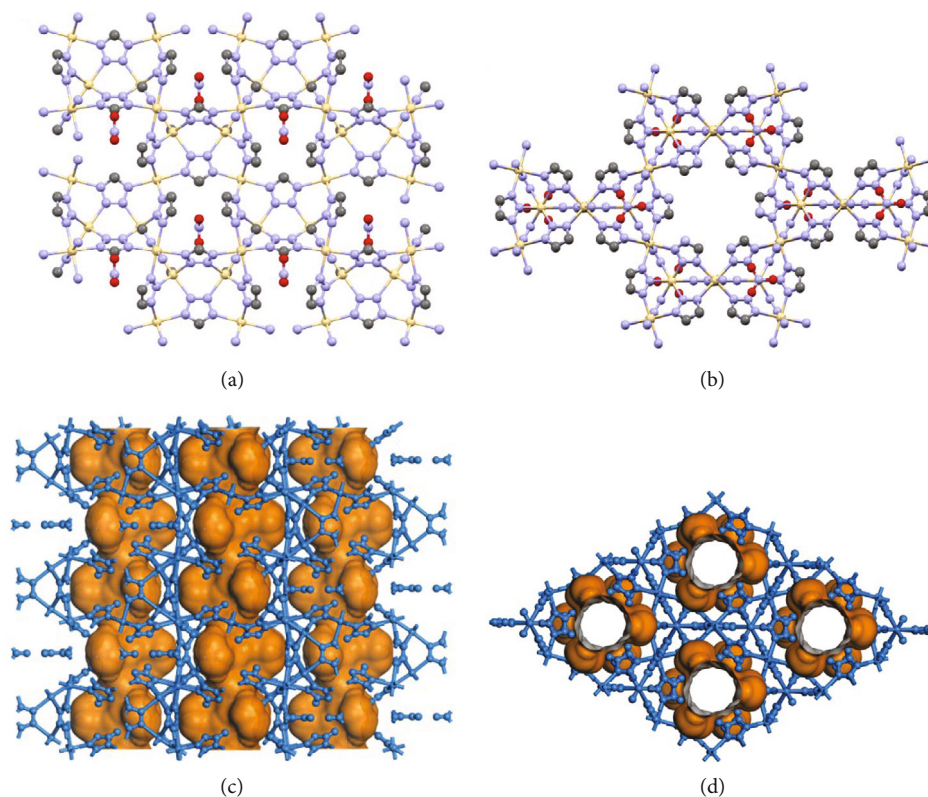
(a)

(b)

(c)

(d)

FIGURE 1: The framework of Cd-TZ without hydrogen atoms and solvent molecules viewed along the *a* axis (a) and *b* axis (b) (Cd, C, N, and O are represented by light yellow, gray, lavender, and red, respectively). The pore structure of Cd-TZ without hydrogen atoms and solvent molecules viewed along the *a* axis (c) and *b* axis (d).
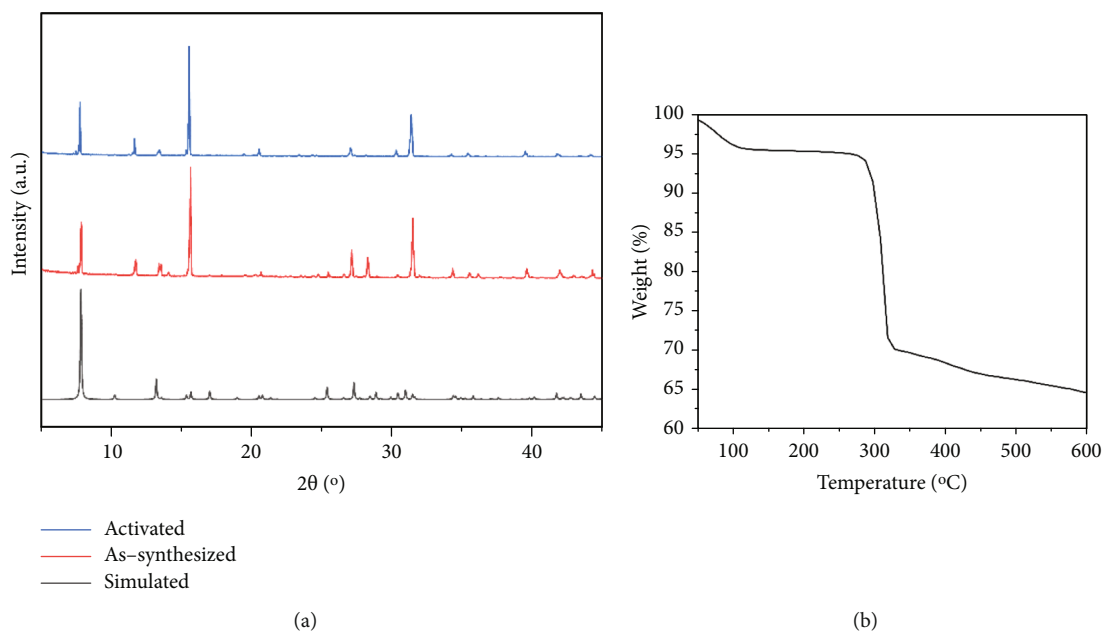

(a)

(b)

FIGURE 2: (a) PXRD patterns of as-synthesized Cd-TZ and activated Cd-TZ and (b) thermogravimetry curves of Cd-TZ.

superior to some of the benchmark MOFs like SIFSIX-21-Ni (7.8) [39], TIFSIX-2-Cu-i (6.5) [40], FJU-90a (4.3) [41], and ZrT-1-tetrazl (2.8) [42] under similar conditions. As shown in Figure S10, the selectivity of Cd-TZ for the binary mixtures of C_2H_2/C_2H_4 (50/50, *v/v*) is up to 20.1 at 273 K and 1 bar, with the temperature increasing to 298 K, and
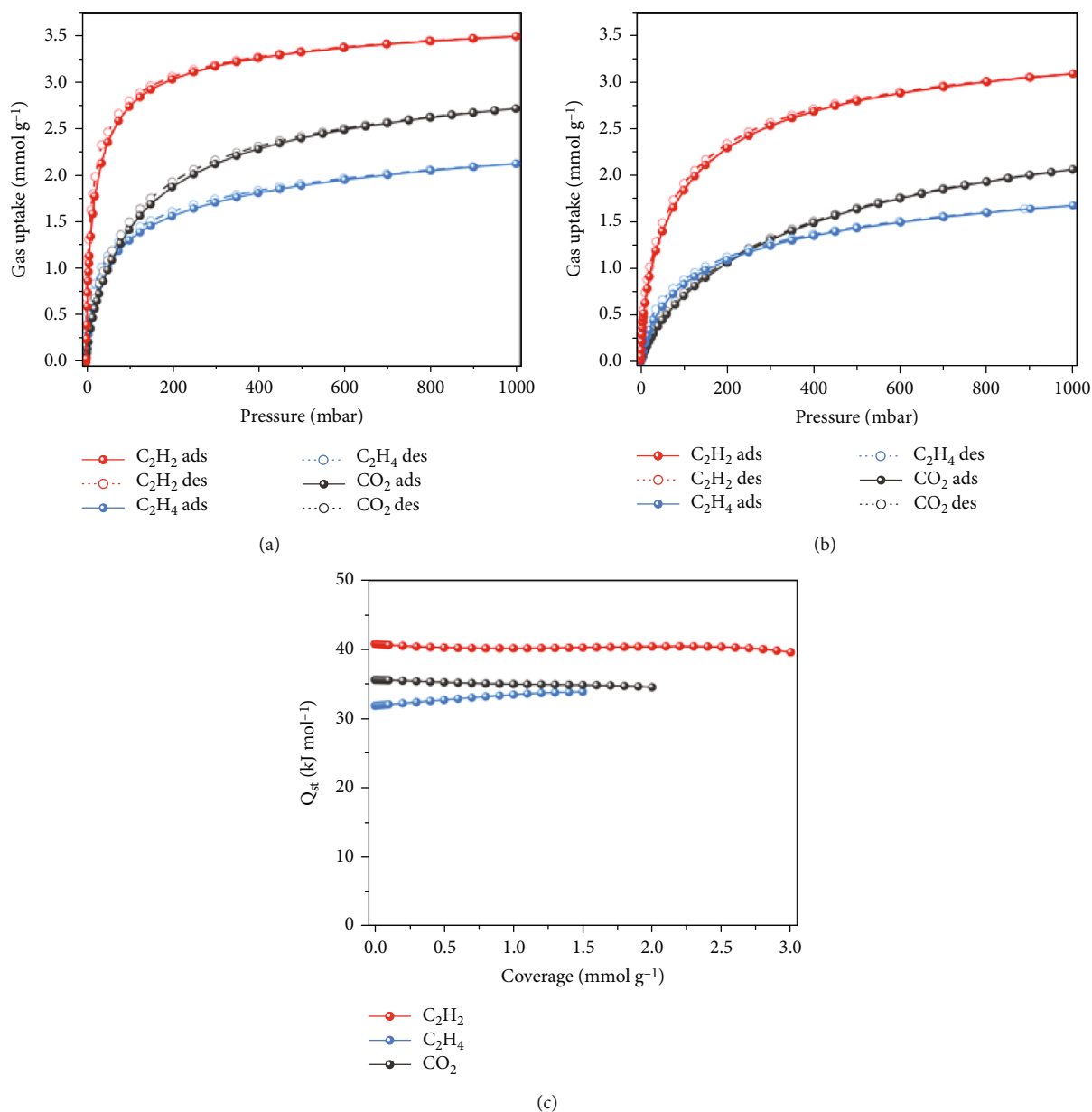
(a)

(b)

(c)

FIGURE 3: Single-component adsorption-desorption isotherms of C_2H_2, CO_2, and C_2H_4 in Cd-TZ at (a) 273 K and (b) 298 K. (c) The isosteric enthalpies of adsorption for C_2H_2, CO_2, and C_2H_4 in Cd-TZ.

the selectivity is about 13.3, which surpasses most of the reported MOFs, such as cPAF-28 (12.2) [43], MUF-17 (8.73) [30], NbU-1 (5.9) [44], CuTiF$_6$-TPPY (5.47) [45], and Fe-MOF-74 (2.1) [46]. Consider that C_2H_2 is a minor impurity in the crude C_2H_4 production by the cracking of ethane. Therefore, the IAST selectivity of C_2H_2/C_2H_4 (1/99, v/v) was also calculated in addition to that of C_2H_2/C_2H_4 (50/50, v/v). The calculated IAST selectivity value for the binary mixtures of C_2H_2/C_2H_4 (1/99, v/v) is 7.3 higher than those of SIFSIX-3-Ni (5.0) [47] and NUM-11a (1.65) [48]. These calculation results further indicate that Cd-TZ is a potential porous material in separating C_2H_2/CO_2 and removing C_2H_2 from C_2H_4.

The optimal adsorption sites of C_2H_2, C_2H_4, and CO_2 in the framework of Cd-TZ were elucidated by DFT calcula-

tions. The calculated static binding energy of C_2H_2 in Cd-TZ is 75.1 kJ mol^{-1}, much higher than those of C_2H_4 with 54.4 kJ mol^{-1} and CO_2 with 35.6 kJ mol^{-1}. The lowest-energy binding configuration of C_2H_2, C_2H_4, and CO_2 in Cd-TZ is shown in Figure 4, indicating that the adsorbed C_2H_2 molecule is trapped in the center of the cavity and strongly interacts with the surrounding N atoms, which are highly electronegative. Figure S11 shows that the optimized distance between one H atom of C_2H_2 and the noncoordinated N atom in the cavity is 2.14 Å, which is smaller than the sum of the van der Waals radius of the H atom (1.20 Å) and N atom (1.55 Å). Moreover, the calculated distances between C atoms of C_2H_2 and H atoms of tetrazole are 2.72 Å and 2.74 Å, respectively, shorter than the sum of the van der Waals radius of H
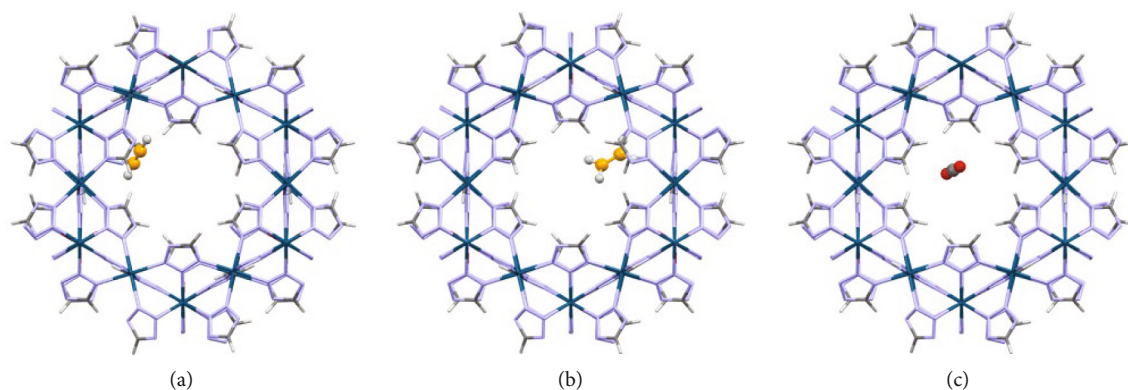
(a)   (b)   (c)

FIGURE 4: Comparison of the optimal (a) C_2H_2, (b) C_2H_4, and (c) CO_2 adsorption sites observed by DFT calculations along the b axis. Cd, C, N, and H in Cd-TZ are represented by dark blue, bright grey, lavender, and white, respectively. C in C_2H_2 and C_2H_4 is represented by bright yellow.
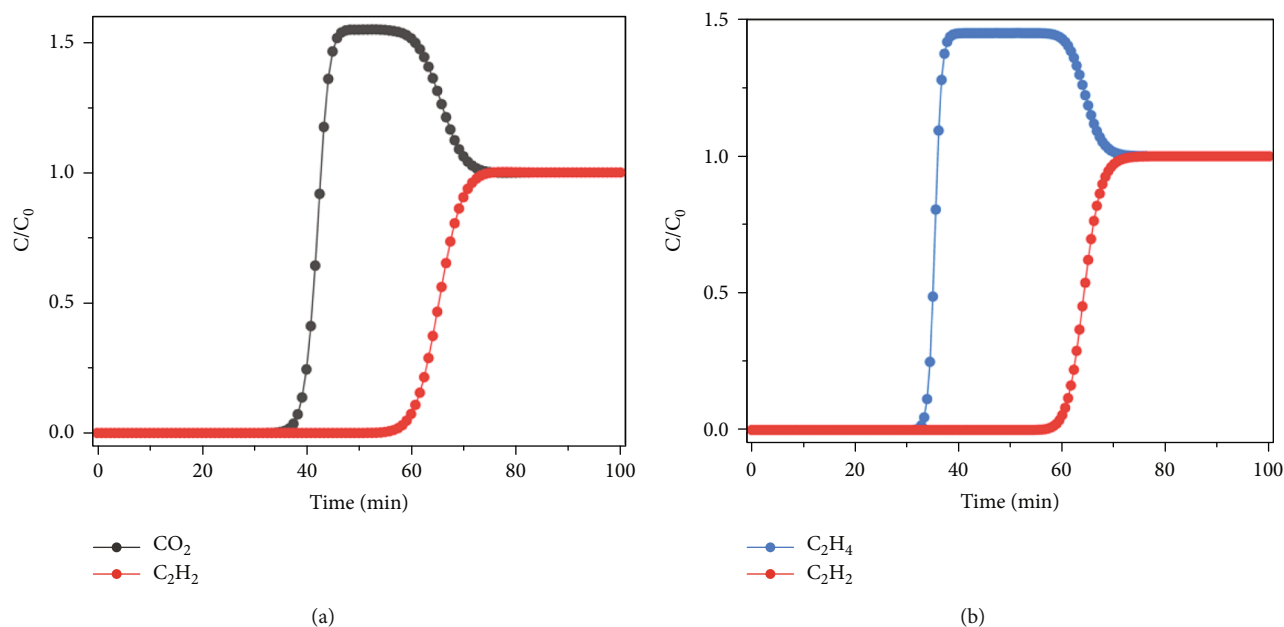

(a)   (b)

FIGURE 5: Simulated breakthrough curves for (a) C_2H_2/CO_2 (50/50, v/v) and (b) C_2H_2/C_2H_4 (50/50, v/v) at 298 K and 1 bar.

and C atoms, 2.90 Å. These results indicate the robust affinity of the framework to the C_2H_2 molecules. C_2H_4 has a larger size and planar configuration. Thus, only one end of the $=CH_2$ group is adsorbed in the cavity with side-on orientation and forms a weaker interaction with the surrounding tetrazoles (Figure S12). There are four C=C-H⋯N dipolar interactions (2.89 Å, 2.92 Å, 3.10 Å, and 3.10 Å) observed between C_2H_4 and the tetrazoles in the cavity. And the calculated H-C=C⋯H distances between C_2H_4 and the tetrazoles in the cavity are 2.70~2.89 Å (2.70 Å, 2.73 Å, 2.87 Å, and 2.89 Å). As shown in Figure S13, CO_2 has two weak C_{CO2}⋯N interactions and three weak O_{CO2}⋯H interactions with the tetrazoles. The calculated distance of C_{CO2}⋯N is 3.40 Å and 3.47 Å, while the estimated distance of O_{CO2}⋯H is 2.85 Å, 3.41 Å, and 3.49 Å, indicating the weak interaction between CO_2 and the framework. The simulation calculations confirm that

the adsorption affinity of C_2H_2 is much stronger than C_2H_4 and CO_2, consistent with the experimental results.

The separation performance of Cd-TZ was investigated by breakthrough simulations with the binary gas mixture of C_2H_2/CO_2 (50/50, v/v) and C_2H_2/C_2H_4 (50/50, v/v) at 298 K and 1 bar. As shown in Figure 5(a), CO_2 gas was first eluted at 31 min from the column, whereas C_2H_2 was retained in the column until 50 min, demonstrating a stronger binding affinity of the framework to C_2H_2 molecules. Figure 5(b) shows that Cd-TZ can realize the complete separation of C_2H_2/C_2H_4 (50/50, v/v). The C_2H_4 broke through from the column after 30 minutes, and no C_2H_2 was eluted out before 53 minutes, indicating that high-purity C_2H_4 could be obtained with the framework. All the above results demonstrate the great potential of Cd-TZ in the separation of C_2H_2/CO_2 and C_2H_2/C_2H_4 in practice.

4. Conclusions

In summary, we have investigated the N-rich cage-based microporous metal-organic framework, Cd-TZ, showing a stronger affinity for C_2H_2 than CO_2 and C_2H_4, and efficiently separating binary mixtures of C_2H_2/CO_2 and C_2H_2/C_2H_4. Owing to the abundant uncoordinated nitrogen atoms on the pore surface and the cavities, Cd-TZ exhibits a high capacity for C_2H_2 (3.10 mmol g^{-1} at 298 K and 1 bar). The calculated IAST selectivity of Cd-TZ for C_2H_2/CO_2 and C_2H_2/C_2H_4 is 8.3 and 13.3, respectively. The breakthrough simulation results well confirm the separation performance of Cd-TZ. In addition, the preferential binding of C_2H_2 over CO_2 and C_2H_4 is clearly demonstrated by DFT calculations. This study provides an exquisite example of MOF possessing abundant electronegative nitrogen sites on the pore surfaces and the cavities for the challenging separation of C_2H_2/CO_2 and C_2H_2/C_2H_4.

Data Availability

The data used to support the findings of this study are available from the corresponding authors upon request. In addition, all of the experimental datasets are available from the online Zenodo repository (10.5281/zenodo.7645931) [49].

Conflicts of Interest

The authors declare that they have no conflicts of interest.

Acknowledgments

Supplementary Materials

Figure S1-S2: the specific surface area calculations of Cd-TZ. Figure S3-S5: C_2H_2, C_2H_4, and CO_2 isotherm fittings using the virial method. Figure S6-S8: C_2H_2, C_2H_4, and CO_2 isotherm fittings using the DSLF equation. Figure S9-S10: IAST adsorption selectivity for C_2H_2/CO_2 and C_2H_2/C_2H_4. Figure S11-S13: the optimal adsorption sites of C_2H_2, C_2H_4, and CO_2 in Cd-TZ. (Supplementary Materials)

References

[1] S. Mukherjee, D. Sensharma, K.-J. Chen, and M. J. Zaworotko, "Crystal engineering of porous coordination networks to enable separation of C_2 hydrocarbons," *Chemical Communications*, vol. 56, no. 72, pp. 10419–10441, 2020.

[2] H. Schobert, "Production of acetylene and acetylene-based chemicals from coal," *Chemical Reviews*, vol. 114, no. 3, pp. 1743–1760, 2014.

[3] Y. Chai, X. Han, W. Li et al., "Control of zeolite pore interior for chemoselective alkyne/olefin separations," *Science*, vol. 368, no. 6494, pp. 1002–1006, 2020.

[4] H. Zimmermann and R. Walzl, "Ethylene," in *Ullmann's Encyclopedia of Industrial Chemistry*, Wiley-VCH Publishing, 2009.

[5] T. Ren, M. Patel, and K. Blok, "Olefins from conventional and heavy feedstocks: energy use in steam cracking and alternative processes," *Energy*, vol. 31, no. 4, pp. 425–451, 2006.

[6] S. Kitagawa, R. Kitaura, and S. Noro, "Functional porous coordination polymers," *Angewandte Chemie International Edition*, vol. 43, no. 18, pp. 2334–2375, 2004.

[7] B.-Y. Zhu, T. Zhang, C.-H. Li et al., "A (3,8)-connected metal-organic framework with bending dicarboxylate linkers for C_2H_2/CO_2 separation," *Inorganic Chemistry*, vol. 61, no. 11, pp. 4555–4560, 2022.

[8] Y. Deng, Q. Mao, S. Luo, X. Xie, and L. Luo, "Adsorption-based removal of Sb (III) from wastewater by graphene oxide-modified zirconium-based metal-organic framework composites," *Adsorption Science & Technology*, vol. 2022, article 9222441, pp. 1–13, 2022.

[9] K. Wang, Y. Li, L.-H. Xie, X. Li, and J.-R. Li, "Construction and application of base-stable MOFs: a critical review," *Chemical Society Reviews*, vol. 51, no. 15, pp. 6417–6441, 2022.

[10] F. G. Quintero-Alvarez, C. K. Rojas-Mayorga, D. I. Mendoza-Castillo, I. A. Aguayo-Villarreal, and A. Bonilla-Petriciolet, "Physicochemical modeling of the adsorption of pharmaceuticals on MIL-100-Fe and MIL-101-Fe MOFs," *Adsorption Science & Technology*, vol. 2022, article 4482263, pp. 1–14, 2022.

[11] J.-W. Wang, S.-C. Fan, H.-P. Li, X. Bu, Y.-Y. Xue, and Q.-G. Zhai, "De-linker-enabled exceptional volumetric acetylene storage capacity and benchmark C_2H_2/C_2H_4 and C_2H_2/CO_2 separations in metal–organic frameworks," *Angewandte Chemie International Edition*, vol. 62, no. 10, 2023.

[12] Z. Zhang, P. Li, T. Zhao, and Y. Xia, "Enhanced CO_2 adsorption and selectivity of CO_2/N_2 on amine@ZIF-8 materials," *Adsorption Science & Technology*, vol. 2022, article 3207986, pp. 1–12, 2022.

[13] J.-R. Li, R. J. Kuppler, and H.-C. Zhou, "Selective gas adsorption and separation in metal-organic frameworks," *Chemical Society Reviews*, vol. 38, no. 5, pp. 1477–1504, 2009.

[14] J.-R. Li, J. Sculley, and H.-C. Zhou, "Metal-organic frameworks for separations," *Chemical Reviews*, vol. 112, no. 2, pp. 869–932, 2012.

[15] R.-B. Lin, L. Li, H.-L. Zhou et al., "Molecular sieving of ethylene from ethane using a rigid metal-organic framework," *Nature Materials*, vol. 17, no. 12, pp. 1128–1133, 2018.

[16] H. Li, L. Li, R.-B. Lin et al., "Porous metal-organic frameworks for gas storage and separation: status and challenges," *EnergyChem*, vol. 1, no. 1, article 100006, 2019.

[17] K.-J. Chen, D. G. Madden, S. Mukherjee et al., "Synergistic sorbent separation for one-step ethylene purification from a four-component mixture," *Science*, vol. 366, no. 6462, pp. 241–246, 2019.

[18] Q. Dong, X. Zhang, S. Liu et al., "Tuning gate-opening of a flexible metal–organic framework for ternary gas sieving separation," *Angewandte Chemie International Edition*, vol. 59, no. 50, pp. 22756–22762, 2020.

[19] Z. Xu, X. Xiong, J. Xiong et al., "A robust Th-azole framework for highly efficient purification of C_2H_4 from a $C_2H_4/C_2H_2/C_2H_6$ mixture," *Nature Communications*, vol. 11, no. 1, p. 3163, 2020.

[20] X. Zhang, J.-X. Wang, L. Li et al., "A rod-packing hydrogen-bonded organic framework with suitable pore confinement for benchmark ethane/ethylene separation," *Angewandte Chemie International Edition*, vol. 60, no. 18, pp. 10304–10310, 2021.

[21] Y. Yang, L. Li, R.-B. Lin et al., "Ethylene/ethane separation in a stable hydrogen-bonded organic framework through a gating mechanism," *Nature Chemistry*, vol. 13, no. 10, pp. 933–939, 2021.

[22] Y. Wang, C. Hao, W. Fan et al., "One-step ethylene purification from an acetylene/ethylene/ethane ternary mixture by cyclopentadiene cobalt-functionalized metal–organic frameworks," *Angewandte Chemie International Edition*, vol. 60, no. 20, pp. 11350–11358, 2021.

[23] J.-W. Cao, S. Mukherjee, T. Pham et al., "One-step ethylene production from a four-component gas mixture by a single physisorbent," *Nature Communications*, vol. 12, no. 1, p. 6507, 2021.

[24] T. Zhang, J.-W. Cao, S.-Y. Zhang et al., "General pore features for one-step C_2H_4 production from a C_2 hydrocarbon mixture," *Chemical Communications*, vol. 58, no. 32, pp. 4954–4957, 2022.

[25] C. E. Webster, R. S. Drago, and M. C. Zerner, "Molecular dimensions for adsorptives," *Journal of the American Chemical Society*, vol. 120, no. 22, pp. 5509–5516, 1998.

[26] R.-B. Lin, L. Li, H. Wu et al., "Optimized separation of acetylene from carbon dioxide and ethylene in a microporous material," *Journal of the American Chemical Society*, vol. 139, no. 23, pp. 8022–8028, 2017.

[27] M. Jiang, X. Cui, L. Yang et al., "A thermostable anion-pillared metal-organic framework for C_2H_2/C_2H_4 and C_2H_2/CO_2 separations," *Chemical Engineering Journal*, vol. 352, pp. 803–810, 2018.

[28] J. Lee, C. Y. Chuah, J. Kim et al., "Separation of acetylene from carbon dioxide and ethylene by a water-stable microporous metal–organic framework with aligned imidazolium groups inside the channels," *Angewandte Chemie International Edition*, vol. 57, no. 26, pp. 7869–7873, 2018.

[29] L.-N. Ma, Z.-H. Wang, L. Zhang, L. Hou, Y.-Y. Wang, and Z. Zhu, "Extraordinary Separation of Acetylene-Containing Mixtures in a Honeycomb Calcium-Based MOF with Multiple Active Sites," *ACS Applied Materials & Interfaces*, vol. 15, no. 2, pp. 2971–2978, 2023.

[30] O. T. Qazvini, R. Babarao, and S. G. Telfer, "Multipurpose metal-organic framework for the adsorption of acetylene: ethylene purification and carbon dioxide removal," *Chemistry of Materials*, vol. 31, no. 13, pp. 4919–4926, 2019.

[31] Y. Du, Y. Chen, Y. Wang et al., "Optimized pore environment for efficient high selective C_2H_2/C_2H_4 and C_2H_2/CO_2 separation in a metal-organic framework," *Separation and Purification Technology*, vol. 256, article 117749, 2021.

[32] D.-C. Zhong, J.-B. Lin, W.-G. Lu, L. Jiang, and T.-B. Lu, "Strong hydrogen binding within a 3D microporous metal-organic framework," *Inorganic Chemistry*, vol. 48, no. 18, pp. 8656–8658, 2009.

[33] L. Yang, A. Jie, L. Ge, X. Cui, and H. Xing, "A novel interpenetrated anion-pillared porous material with high water tolerance afforded efficient C_2H_2/C_2H_4 separation," *Chemical Communications*, vol. 55, no. 34, pp. 5001–5004, 2019.

[34] Y.-L. Peng, T. Pham, P. Li et al., "Robust ultramicroporous metal–organic frameworks with benchmark affinity for acetylene," *Angewandte Chemie International Edition*, vol. 57, no. 34, pp. 10971–10975, 2018.

[35] Q. Ding, Z. Zhang, Y. Liu, K. Chai, R. Krishna, and S. Zhang, "One-step ethylene purification from ternary mixtures in a metal–organic framework with customized pore chemistry and shape," *Angewandte Chemie International Edition*, vol. 61, no. 35, article e202208134, 2022.

[36] L. Yang, L. Yan, Y. Wang et al., "Adsorption site selective occupation strategy within a metal–organic framework for highly efficient sieving acetylene from carbon dioxide," *Angewandte Chemie International Edition*, vol. 60, no. 9, pp. 4570–4574, 2021.

[37] L. Yang, L. Yan, W. Niu et al., "Adsorption in reversed order of C_2 hydrocarbons on an ultramicroporous fluorinated metal-organic framework," *Angewandte Chemie International Edition*, vol. 61, no. 25, article e202204046, 2022.

[38] F. Luo, C. Yan, L. Dang et al., "UTSA-74: a MOF-74 isomer with two accessible binding sites per metal center for highly selective gas separation," *Journal of the American Chemical Society*, vol. 138, no. 17, pp. 5678–5684, 2016.

[39] N. Kumar, S. Mukherjee, N. C. Harvey-Reid et al., "Breaking the trade-off between selectivity and adsorption capacity for gas separation," *Chem*, vol. 7, no. 11, pp. 3085–3098, 2021.

[40] K.-J. Chen, H. S. Scott, D. G. Madden et al., "Benchmark C_2H_2/CO_2 and CO_2/C_2H_2 separation by two closely related hybrid ultramicroporous materials," *Chem*, vol. 1, no. 5, pp. 753–765, 2016.

[41] Y. Ye, Z. Ma, R.-B. Lin et al., "Pore space partition within a metal-organic framework for highly efficient C_2H_2/CO_2 separation," *Journal of the American Chemical Society*, vol. 141, no. 9, pp. 4130–4136, 2019.

[42] W. Fan, S. B. Peh, Z. Zhang et al., "Tetrazole-functionalized zirconium metal-organic cages for efficient C_2H_2/C_2H_4 and C_2H_2/CO_2 separations," *Angewandte Chemie International Edition*, vol. 60, no. 32, pp. 17338–17343, 2021.

[43] S. Zhou, Z. Liu, P. Zhang et al., "Tailoring the pore chemistry in porous aromatic frameworks for selective separation of acetylene from ethylene," *Chemical Science*, vol. 13, no. 37, pp. 11126–11131, 2022.

[44] J. Li, L. Jiang, S. Chen et al., "Metal-organic framework containing planar metal-binding sites: efficiently and cost-effectively enhancing the kinetic separation of C_2H_2/C_2H_4," *Journal of the American Chemical Society*, vol. 141, no. 9, pp. 3807–3811, 2019.

[45] P. Zhang, Y. Zhong, Y. Zhang et al., "Synergistic binding sites in a hybrid ultramicroporous material for one-step ethylene purification from ternary C_2 hydrocarbon mixtures," *Science Advances*, vol. 8, no. 23, 2022.

[46] E. D. Bloch, W. L. Queen, R. Krishna, J. M. Zadrozny, C. M. Brown, and J. R. Long, "Hydrocarbon separations in a metal-organic framework with open iron(II) coordination sites," *Science*, vol. 335, no. 6076, pp. 1606–1610, 2012.

[47] X. Cui, K. Chen, H. Xing et al., "Pore chemistry and size control in hybrid porous materials for acetylene capture from ethylene," *Science*, vol. 353, no. 6295, pp. 141–144, 2016.

[48] S.-Q. Yang, L. Zhou, Y. He et al., "Two-dimensional metal-organic framework with ultrahigh water stability for separation of acetylene from carbon dioxide and ethylene," *ACS Applied Materials & Interfaces*, vol. 14, no. 29, pp. 33429–33437, 2022.

[49] L. Yang and X. Zhao, *Highly Selective Separation of C_2H_2/CO_2 and C_2H_2/C_2H_4 in an N-Rich Cage-Based Microporous Metal-Organic Framework*, Zenodo, 2023.